

# A Conceptual Design Study of a Compact Photon Source (CPS) for Jefferson Lab

E. Chudakov,<sup>1</sup> D. Day,<sup>2</sup> P. Deltiarenko,<sup>1</sup> R. Ent,<sup>1</sup> D.J. Hamilton,<sup>3</sup> T. Horn,<sup>4,1,\*</sup> D. Keller,<sup>2</sup> C. Keppel,<sup>1</sup> G. Niculescu,<sup>5</sup> P. Reid,<sup>6</sup> I. Strakovsky,<sup>7</sup> B. Wojtsekhowski,<sup>1</sup> and J. Zhang<sup>2</sup>

<sup>1</sup>*Jefferson Lab*

<sup>2</sup>*University of Virginia*

<sup>3</sup>*University of Glasgow*

<sup>4</sup>*Catholic University of America*

<sup>5</sup>*James Madison University*

<sup>6</sup>*Saint Mary's University*

<sup>7</sup>*George Washington University*

(Dated: September 15, 2019)

This document describes the technical design concept of a compact high intensity photon source (CPS) to be used with targets polarized using the dynamic nuclear polarization technique. The novel CPS technique unlocks access to physics processes with very small scattering probabilities which is not possible with currently existing facilities. Capable of producing  $10^{12}$  equivalent photons per second, the deployment of the CPS will result in a large gain in polarized experiment figure-of-merit (by a factor of  $\sim 30$ ). Compared to a traditional bremsstrahlung photon source the proposed concept will present several advantages, including much lower radiation levels, both prompt and post-operational due to the beam line elements radio-activation. For use with polarized targets, the heat load and radiation damage effects present no special burden.

Keywords: photon source

## I Introduction

Gaining a quantitative description of the nature of strongly bound systems is of great importance for our understanding of the fundamental structure and origin of matter. One of the most promising ways to access information on the dynamical structure of the nucleon is through exclusive reactions at high momentum transfer, in which the deep interior of the nucleon is studied with a highly-energetic photon or electron probe and all final-state particles are detected. Even though the scattering probability of such reactions is extremely small <sup>1</sup> it has become clear that such reactions offer a promising route to imaging of the elusive 3-D nucleon substructure. Indeed, there have been increasingly sophisticated theoretical efforts to exploit the richness of exclusive reactions at short resolution scales.

Exclusive measurements with high-energy electron and photon beams form the core of the new paradigm for sub-atomic science termed "nuclear femtography". In both photon and electron scattering experiments, the scale of the associated imaging that can be performed is set by the invariant squared four-momentum transferred to the proton target,  $-t$ , and the total centre-of-mass energy squared,  $s$ . Measurements over a wide range of  $s$  and  $-t$  with these probes allow for the disentangling of four functions representing the vector, axial, tensor, and pseudo-scalar response of the nu-

cleon. Simultaneous experimental access to all of these functions is most readily achieved by polarizing the nuclear system under study.

Much progress imaging nucleon structure can be made with electron-scattering reactions. Yet, experiments utilizing high-energy photons play a unique complementary role. But, to measure the small scattering probabilities related to exclusive reactions demands high-intensity photon beams. Further, our basic understanding will be much strengthened by imaging longitudinally-polarized <sup>2</sup> and transversely-polarized nucleons. It is for this combination that the proposed concept is so unique: with a new-developed Compact Photon Source (CPS) and a dynamically-nuclear polarized target system, a gain of a factor of 30 in the figure-of-merit (as defined by the photon intensity and the average target polarization over the experiment) can be achieved. This gain could be further doubled by use of a novel magnet system to polarize targets with much larger particle detection acceptance than previously possible. The net gain makes it possible to measure the very small scattering cross sections associated with a new suite of high-energy photon scattering experiments to image and understand the dynamical nucleon structure. The concept of a CPS also enables other science possibilities, like using the source to create a beam of neutral kaons for a new family of hadron spectroscopy experiments. [1]

This document is organized as follows. In

\*Contact email:[hornt@cua.edu](mailto:hornt@cua.edu)

<sup>1</sup> It is much more likely for the highly energetic electron probe to break the proton than leave it intact

<sup>2</sup> along the photon beam direction

section II, we give a short overview of the possible science gain enabled by the CPS, using two examples. In section III, we outline the generic idea behind the novel CPS design as compared to the more traditional photon beam methods. In section IV, the conceptual design and component details of the CPS are presented. Section V lists the requirements a CPS has to meet to fulfill operational dose rates at Jefferson Lab. In section VI, we discuss the results of our shielding design and optimization studies and compare them with the requirements in section V. Finally, section VII deals with engineering and safety aspects including material considerations, and section VIII summarizes the Compact Photon Source design features and performance.

## II Science Opportunities with CPS

Investigating the three-dimensional structure of the nucleon has been an active and productive field of research especially during the last two decades since the invention of the Generalized Parton Distributions (GPD) formalism. Studies towards this three-dimensional structure, or nuclear femtography, continue to be central to the hadron physics program at facilities like Jefferson Lab. The GPD formalism provides a unified description of many important reactions including elastic electron scattering, Deep-Inelastic Scattering (DIS), Deeply-Virtual and Timelike Compton Scattering (DVCS and TCS), Deeply-Virtual Meson Production (DVMP), and Wide-Angle Real Compton Scattering (RCS) and meson production. All of these can be described by a single set of four functions  $H$ ,  $\tilde{H}$ ,  $E$  and  $\tilde{E}$ , which need to be modeled and constrained with parameters extracted from experimental data.

The CPS science program enables studies of the three-dimensional structure of the nucleon, complementary to those with electron beams, and currently features one fully approved and two conditionally approved experiments[1–3].

E12-17-008 [2] will measure polarization observables in Real Compton Scattering. This is a fundamental and basic process, yet its mechanism in the center-of-mass energy regime of  $\sqrt{s} = 5\text{-}10 \text{ GeV}$  remains poorly understood. Measurements show that these data cannot be described by perturbative calculations involving the scattering of three valence quarks, but that the dominant mechanism could be the so-called "handbag model" where the photon scatters from a single active quark, and convoluted with a coupling of this struck quark to the spectator system is described by GPDs. It is this latter conceptual mechanism that lies at the root of the worldwide efforts of 3D (spatial) imaging of the proton's quark-gluon substructure, as the GPDs contain information about the transverse spatial distribution of quarks and their longitudinal momenta inside the proton.

The RCS experimental observables provide several constraints for GPDs which are complementary to other exclusive reactions due to an  $e_a^2$  factor and an additional  $1/x$  weighting in the GPD integrals for RCS. For example, the elastic form factor  $F_1(t) = \sum_a e_a \int dx H^a(x, 0, t)$  is related to the RCS vector form factor  $R_V(t) = \sum_a e_a^2 \int \frac{dx}{x} H^a(x, 0, t)$ , both of which are based on the same underlying GPD  $H(x, 0, t)$ . Similarly, polarized observables in RCS uniquely provide high  $-t$  constraints on  $\tilde{H}(x, \xi, t)$  via extraction of the RCS axial form factor  $R_A(t)$  in a kinematic regime where precise data on the nucleon axial form factor is not available. A measurement of the spin asymmetry in RCS with the proton target longitudinally polarized can further disentangle the various handbag mechanisms. If consistent with the measurement of the spin transfer from the photon to the scattered proton, the asymmetry can indeed be surprisingly large and stable with respect to the photon center-of-mass scattering angle. Such investigations into the mechanisms behind RCS will provide crucial insight into the nature of exclusive reactions and proton structure and are ideally suited for the facilities provided by the Jefferson Lab 12-GeV upgrade.

C12-18-005 [3] will probe 3D nucleon structure through Timelike Compton Scattering, where a real photon is scattered off a quark in the proton and a high-mass (virtual) photon is emitted, then decays into a lepton pair. Using a transversely polarized proton target and a circularly polarized photon beam, we can access several independent observables directly sensitive to the GPDs, and in particular the GPD  $E$  which is poorly constrained and of great interest due to its relation with the orbital momentum of the quarks. We plan to measure the unpolarized scattering probabilities or cross section, the cross section using circularly polarized photon beam, and the cross sections using transversely-polarized protons. This provides a first fundamental test of the universality of the GPDs, as the GPDs extracted from TCS should be comparable with those that will be extracted from the analogous spacelike (electron) scattering process - Deeply Virtual Compton Scattering, a flagship program of the 12-GeV Jefferson Lab Upgrade.

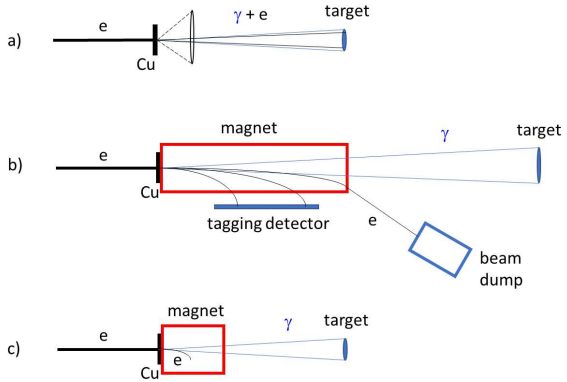


Figure 1: *Different schemes to produce high-energy photon beams. Scheme a) is the traditional bremsstrahlung technique where a Cu radiator is placed in an electron beam to render a mixed photon and electron beam. In scheme b) a deflection magnet and beam dump are used to peel off the electrons and produce a photon-only beam. Scheme c) is the new Compact Photon Source technique, with a compact combined magnet-electron dump and a narrow photon-only beam.*

### III Science Method

A traditional source of high-energy photons comes from an electron beam hitting a radiator, most commonly copper, producing a cone of bremsstrahlung photons accompanying the electron beam (see Fig. 1a). The spread in the photon and outgoing electron beams is dominated by electron multiple scattering, and for electron beam energies of a few GeV is typically less than 1 mrad. Accompanying this mixed photon and electron beam is a much larger angular distribution of secondary particles produced in the electron-nuclei shower. For example, the cone of secondary particles that survive filtering through a heavy absorber material of one nuclear interaction length ( $\approx 140-190 \text{ g/cm}^2$  or  $\approx 15 \text{ cm}$ ) has an angular spread of 100-1000 mrad. Even if this method can produce the largest flux of photons, drawbacks are that the beam is a mix of photons and electrons, that the photon beam energy is not a priori known, and that the method is accompanied with large radiation background doses due to the large spread of secondary particles produced.

An alternate method to produce a (pure) photon beam includes a radiator, a deflection magnet and a beam dump for the undeflected electrons, augmented for energy-tagged photon beams with a set of focal plane detectors covering a modest to large momentum acceptance (see Fig. 1b). Such

a configuration requires significant space along the beam direction and heavy shielding around the magnet and the beam dump, which have large openings due to the large angular and energy spread of the electrons after interactions in the radiator. In addition, without tight collimation the traditional scheme leads to a large size of the photon beam at the target due to divergence of the photon beam and the long path from the radiator to the target. This can be an issue as the beam spot size contributes to the angular and momentum reconstruction resolution of the resultant reaction products due to uncertainty in the transverse vertex position. As an example, to obtain the needed reconstruction resolution of the scattered photon in RCS the photon spot size at the target must be equal or less than 2 mm. This would require the target to be at a distance of no more than 2 meters from the radiator, which is often practically impossible. The advantage of this method is that one has a pure photon beam, and if augmented with a set of focal-plane tagging detectors the exact photon energies can be determined. A drawback is that the flux of incident electrons must be modest ( $\approx 100 \text{ nA}$ ) and, correspondingly, the photon flux is less than otherwise might be possible, especially when a tagging method is used. In addition, this scheme comes with appreciable radiation doses, especially with increased photon fluxes, as particles are allowed to propagate over short distances before mitigation of radiation by containments starts to be effective.

The CPS (see Fig. 1c) addresses the shortcomings of these two traditional techniques. The concept of the CPS takes advantage of the modest spread of the photon beam relative to the angular distribution of the secondary particles produced in the electron-nuclei shower. The CPS combines in a single shielded assembly all elements necessary for the production of the intense photon beam and ensures that the operational radiation dose rates around it are acceptable (see Ref. [4]). Much of this is achieved by keeping the overall dimensions of the setup limited, and by careful choice and ordering of materials. The CPS design features a magnet, a central copper absorber to handle the power deposition, and tungsten powder and borated plastic to hermetically shield the induced radiation doses as close to the source as possible. The magnet acts as dump for the electrons with a cone of photons escaping through a small collimator. The size of the collimator can be as narrow as the photon beam size with natural divergence plus the size of the beam raster. The combined magnet-dump thus allows for dramatically reducing the magnet aperture and length, as well as the weight of the radi-

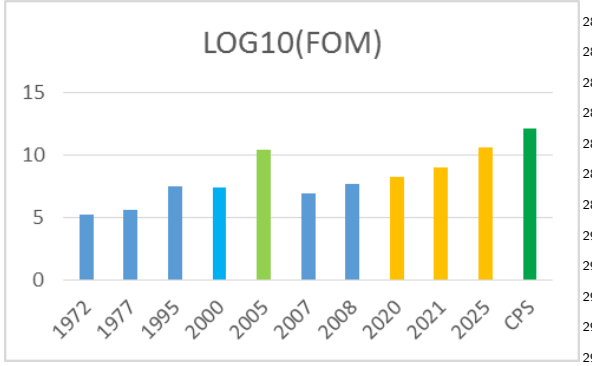


Figure 2: The Figure-Of-Merit (FOM) of photon beam experiments with Dynamically Nuclear Polarized targets, defined as the logarithm of the effective photon beam intensity times the averaged target polarization squared, as a function of time. Note the large gain over a factor of 30 as compared to any setup, enabled by the CPS. The vertical axis is log scale. The indicated FOM in 1972, 1977, 1995, 2007 and 2008 are based on actual experiments at Daresbury, Bonn, Jefferson Lab and Mainz [7–9]. The FOM noted in 2000 and 2005 are based upon proposed setups at SLAC and Jefferson Lab, with the latter closest in concept to the CPS. We also add the projected FOM of approved future experiments at HiGS/Duke and Jefferson Lab.

ation shield, due to the compactness of the source and minimization of openings, thus reducing radiation leakage. This opens a practical way forward with management of both the radiation environment in the magnet and the power deposition density in the copper absorber.

Compared to the more traditional bremsstrahlung photon sources (Figs. 1a and 1b and e.g. Refs. [5, 6]), the proposed solution offers several advantages, including an intense and narrow photon-only beam and much lower radiation levels, both prompt and post-operational from radio-activation of the beam line elements. The drawbacks are a somewhat reduced photon flux as compared to the scheme of Fig. 1(a), and not having with a focal plane detection option the ability to directly measure the photon energy as in the scheme of Fig. 1(b).

The primary gain of the CPS is for experiments using Dynamically Nuclear Polarized (DNP) Targets, with an estimated gain in Figure-Of-Merit of a factor of 30 (see Fig. 2). Dynamic Nuclear Polarization is an effective technique to produce polarized protons. Here, a material containing a large fraction of protons is cooled to low temperatures, <1K, and placed in a strong magnetic field, typically about 5 Tesla. The material is first ‘doped’, either chemically or through irradiation,

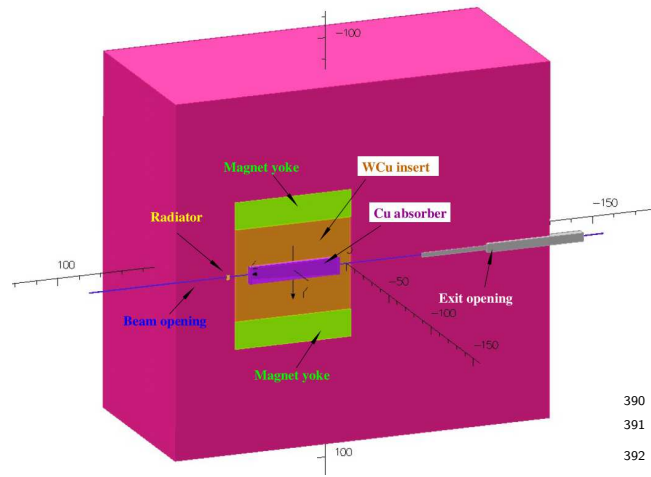
to introduce free radicals (electrons). The low-temperature and high-field conditions cause the electrons to self-polarize, and their polarization is then transferred to the proton using microwave techniques. These conditions however at the same time impose a serious limitation. Beams traversing the polarized target material will produce ionization energy losses warming and depolarizing the target. It also produces other harmful free radicals which allow pathways for proton polarization to decay. This limits the (local) beam intensities the polarized target material can handle.

Conventional target cells have diameters much larger than the desirable beam spot size, and one is forced to minimize rapid degradation of the target polarization by the beam, induced by either heat deposition or ionizing radiation, at one location at the target. The traditional solution of minimizing such localized polarization degradation is fast movement of the beam spot, which allows avoiding overheating of the material and insuring that the depolarizing effects of the beam are uniformly spread over the target volume. A beam raster magnet, which moves the beam with a frequency of several Hz, was used in past experiments in Hall C. However, this does not work for very small apertures, e.g. a few mm by a few mm collimation cone, limiting possible beam motion. The CPS solution for the beam-target raster thus includes a combination of the target rotation around the horizontal axis and  $\pm 10$  mm vertical motion of the target ladder. Such a raster method effectively moves the motion complexity out of the high radiation area of the absorber. The same effect can be achieved by vertical displacement of the beam spot, i.e. by a small variation of the vertical incident angle of the electron beam at the radiator. With a  $\pm 5$  mrad vertical angle variation and 200 cm distance between the radiator and the target, the displacement of the beam spot is equal to  $\pm 1$  cm, about the size of the conventional target cells. Traditionally, such photon beam experiments have been performed using the scheme indicated in Fig. 1a. This limits the electron beam current to less than 100 nA to prevent rapid target polarization damage. With the CPS scheme, we anticipate use of an electron beam current of up to  $2.7 \mu\text{A}$  to provide the photon flux for an equivalent heat load in the DNP target. Hence, we gain a factor of about 30. The history of the figure-of-merit of bremsstrahlung photon beam experiments with DNP targets is further illustrated in Fig. 2.

335 **IV The Compact Photon**  
 336 **Source - Description of**  
 337 **Instrumentation**

338 The physics program described requires a  
 339 high-intensity and narrow polarized photon beam  
 340 and a polarized target to access the exclusive pho-  
 341 toproduction reactions to extract the polarized tar-  
 342 get observables. The CPS provides a compact solu-  
 343 tion with a photon flux of  $1.5 \times 10^{12}$  equivalent pho-  
 344 tons/s, with a factor of 1000 reduction in prompt  
 345 radiation dose compared to a  $2.7 \mu\text{A}$  (30 kW) elec-  
 346 tron beam current striking a 10% Cu radiator. The  
 347 CPS meets the acceptable radiation level require-  
 348 ments for a typical run time of 1000 hours at Jef-  
 349 ferson Lab with the photon source located at 2 m  
 350 from the target. The polarized target requirements  
 351 are fulfilled with a novel rotating polarized target  
 352 cell combined with a dynamic nuclear polarization  
 353 (DNP) system.

354 **A Conceptual Design**



394 Figure 3: The CPS cut-off view. Most of the deflected  
 395 electrons strike a copper absorber, surrounded by a W-  
 396 Cu insert inside the magnet yoke. The outer rectangu-  
 397 lar region in this view is the tungsten-powder shield.

398 The main elements of the CPS are shown  
 399 in Figure 3. Without loss of photon intensity,  
 400 a channel (a collimator for the secondary radiation)  
 401 but not for the photon beam) around the photon  
 402 beam could be as narrow as the photon beam size  
 403 with natural divergence plus the size of the beam  
 404 raster. After passing through the radiator, the  
 405

362 electron beam should be removed from the photon  
 363 line by means of a magnet. The length, aperture  
 364 and field of the magnet are very different in the  
 365 proposed source from the traditional one. In the  
 366 traditional source the magnet is needed to direct  
 367 the electrons to the dump. Because of the large  
 368 momentum spread of electrons which have inter-  
 369 acted in the radiator, the magnet aperture needs  
 370 to be large and the dump entrance should be even  
 371 larger: 13% of the beam power would be lost be-  
 372 fore the beam dump, even with a 10% momentum  
 373 acceptance of the beam line. In contrast, in the  
 374 proposed source the magnet acts as dump for the  
 375 electrons with a cone of photons escaping through  
 376 a small collimator.

377 The electron energy dumping starts on the  
 378 side of the photon beam channel, so a shift of the  
 379 electron trajectory by just 1-3 mm is already suffi-  
 380 cient for the start of the shower. At the same time,  
 381 such a deflection needs to be accomplished at a rel-  
 382 atively short distance (much shorter than the size  
 383 of the radiation shielding) after the beam passes  
 384 through the radiator to keep the source compact.  
 385 Indeed, with a deflection radius,  $R$ , a vertical size  
 386 of the channel,  $2a$ , and a vertical raster size,  $2b$ ,  
 387 the trajectory enters the channel side after trav-  
 388 eling in the magnetic field a distance,  $p$ , which varies  
 389 from  $p = \sqrt{2} R(a - b)$  to  $p = \sqrt{2} R(a + b)$  (see  
 390 the scheme in Figure 4). In the currently proposed

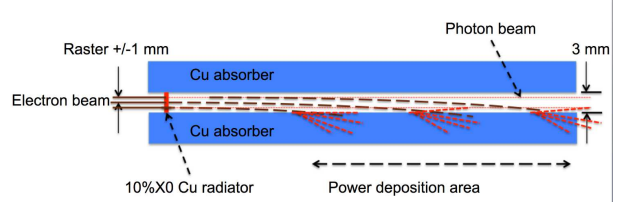


Figure 4: The scheme of beam deflection to the ab-  
 sorber/dump.

390 CPS magnet the trajectory radius  $R$  is about 10 m  
 391 for 11 GeV electrons, the channel size is 0.3 cm,  
 392 and the raster size is 0.2 cm, so the distance  $p$  has  
 393 an average value of 17 cm with a spread of 12 cm.  
 394 A total field integral of 1000 kG-cm is adequate for  
 395 our case, which requires a 50 cm long iron domi-  
 396 nated magnet.

397 This concept of a combined magnet-dump  
 398 allows us to reduce dramatically the magnet aper-  
 399 ture and length, as well as the weight of the radia-  
 400 tion shield, due to the compactness and hermetic-  
 401 ity (with minimized openings) of the system, thus  
 402 significantly reducing the radiation leakage. This  
 403 conceptual approach opens a practical way forward  
 404 for a CPS, providing one can manage both the ra-

406 diation environment in the magnet and the power<sup>437</sup>  
 407 deposition density in the copper absorber.<sup>438</sup>

located. Figure 6 shows the longitudinal profile of the power density according to the MC simulation.

408 B Magnet

Normal conducting magnets for operation in high levels of radiation have been constructed at several hadron facilities, including the neutron spallation source at ORNL and the proton complex JPARC. We designed the magnet with permendur poles tapered in two dimensions, which allows us to reach a strong magnetic field at the upstream end of the magnet (3.2 Tesla or 32 kG), with the coils located 20 cm from the source of radiation. The resulting radiation level at the coil location is calculated to be low enough, below 1 Mrem/hr, to allow the use of a modest-cost kapton tape based insulation of the coils [12]. The length of the magnet was selected to be 50 cm and the field integral 1000 kG-cm. Figure 5 shows the longitudinal profile of the magnetic field obtained from OPERA calculations.

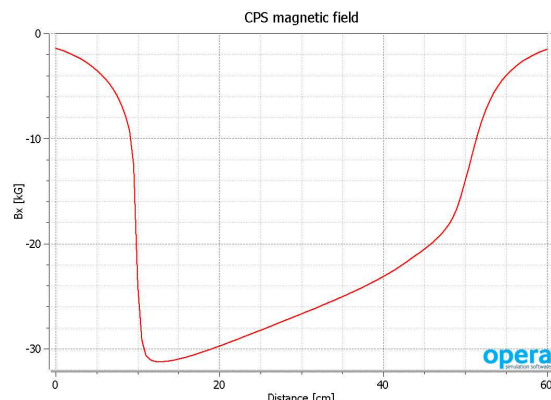


Figure 5: REMOVE "OPERA" FROM FIGURE.  
 Magnetic field ( $B_x$ ) profile along the beam direction,  
 as a distance from the radiator position.

## **426 C Central Absorber**

The beam power is deposited in an absorber<sup>460</sup> made of copper, whose high heat conductivity<sup>461</sup> helps to manage the power density. An absorber<sup>462</sup> made of aluminum would help to reduce power<sup>463</sup> density by a factor of 2-3 compared with copper<sup>464</sup> due to its smaller radiation length, but it would<sup>465</sup> also increase the length of the CPS by about 50 cm<sup>466</sup> so is not preferred. The heat removal from the cop-<sup>467</sup> per absorber is arranged first via heat conduction<sup>468</sup> to the wider area where water cooling tubes are<sup>469</sup>

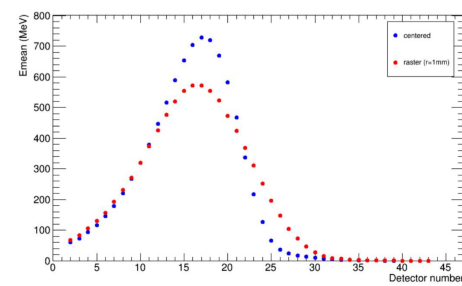


Figure 6: Longitudinal profile of the energy distribution (integrated for one cm copper slab) for a single 11 GeV incident electron. The maximum power density occurs at a distance of 18 cm from the radiator. The blue dots show the energy deposition for the electron beam centered in a 3 mm by 3 mm channel. The red dots show the same for the beam rastered with a radius of one mm.

The transverse distribution of power is also very important to take into account because, for a high energy incident beam, it has a narrow peak. A detailed MC simulation of the deposited power density and the 2-dimensional heat flow analysis were performed to evaluate the maximum temperature in the copper absorber. Figure 7 (left panel) shows the layout of materials in the model used for the temperature analysis. The calculation was performed for the case of a 11 GeV 30 kW beam and a radiator with 10% radiation length thickness, and the temperature was found to be below 400°C, which is well in the acceptable range for copper. Figure 7 (right panel) shows the temperature profile in the transverse plane at the longitudinal location of maximum power deposition. Cooling of the core will require about four gallons of water per minute at 110 psi pressure (at 30°C temperature rise), which is easy to provide.

## D Tungsten-powder Shield

The amount of material needed for radiation shielding is primarily defined by the neutron attenuation length, which is  $30 \text{ g/cm}^2$  for neutrons with energy below 20 MeV and  $125 \text{ g/cm}^2$  for high energy neutrons. The neutron production rate by an electron beam in copper is  $1 \times 10^{12}$  per kW of beam power according to a SLAC report [10] (see Figure 8). At a distance of 16 meters from the unshielded source for a 30 kW beam, the neutron flux would be  $1 \times 10^7 \text{ n/cm}^2/\text{s}$ , which would pro-

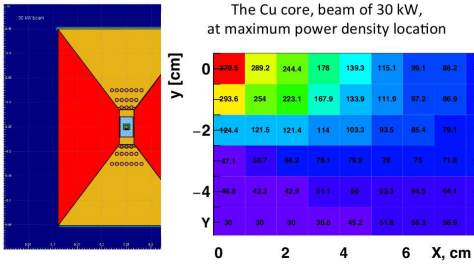


Figure 7: Left panel: the cross section of the absorber<sub>490</sub> (shown in blue (copper) in the center and yellow (W-<sub>491</sub> Cu(20%)) surrounding) with the water cooling chan-<sub>492</sub>nels. Right panel: the temperature map for 1 cm by<sub>493</sub> 1 cm elements at the longitudinal coordinate of the<sub>494</sub> power deposition maximum.

470 duce a radiation level of 110 rem/hr, or 850 times  
471 higher than during the RCS experiment at JLab  
472 (E99-114) (at a 16-meter distance from the pivot  
473 in the upstream direction). The current concep-  
474 tual design with a total shield mass of 850 g/cm<sup>2</sup>  
475 will result in reduction in these radiation levels by  
476 a factor of 1000.

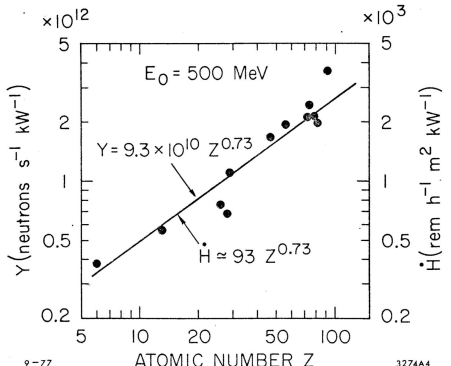


Figure 8: NEED TO MAKE A FIGURE - CANNOT<sub>517</sub> USE THIS ONE SINCE FROM ANOTHER PUBLI-<sub>518</sub>CATION. The neutron yield according to SLAC-PUB<sub>519</sub> 2042 [10].

477 The space inside the magnet between the  
478 poles and coils is filled by an inner copper absorber  
479 and an outer W-Cu(20%) insert, which provides  
480 a good balance between effective beam power ab-  
481 sorption and radiation shielding. For the shield

482 outside the magnet, the current design uses tung-  
483sten powder, whose high density (16.3 g/cm<sup>3</sup>)<sup>3</sup>  
484 helps to reduce the total weight of the device. A  
485 thickness of 50 cm was used as a first iteration  
486 for the thickness of the outer shield of the CPS,  
487 but we have investigated the impact of varying this  
488 amount of outer shielding (as discussed later).

## E Impact on Polarized Target

The most significant gain associated with deployment of the CPS is for experiments using dynamically polarized targets. However, such polarized targets operate with strong 2.5-5 Tesla polarizing fields themselves. In addition, dynamically polarized target operation imposes strict requirements on the field quality at the target location, where fields and gradients need to be compensated at the  $10^{-4}$  level. This necessitates studies of the mutual forces associated with the 2-3 Tesla CPS dipole magnet and the 5 Tesla polarized target solenoid, in terms of both the design of the support structures and the operation of the polarized target.

The fields associated with the combination of these two magnetic systems were calculated using the model shown in Figure 9 (top panel, for the polarized target configured for longitudinal polarization), with the following results obtained:

- When the CPS is ON but the polarized target magnet is OFF, the (total) field at the target location amounts to only about 0.1 Gauss.
- When the polarized target magnet is on and the CPS is OFF or removed, the field at the CPS location is about 130 Gauss.
- When both the CPS is ON and the polarized target magnet is ON, the field gradient at the polarized target center is about 2 Gauss/cm (Figure 10).

These results show that, for the CPS the induced field is mainly due to the CPS magnet yoke becoming polarized by the target field. Whereas for the target, the field gradient at the target location is sufficiently low for routine dynamically polarized NH<sub>3</sub> or ND<sub>3</sub> target operation, with a relative values of  $0.4 \times 10^{-4}$ .

The forces between the polarized target and CPS magnets were calculated by using several methods, including an analytical estimate for the 700 kA per coil (four of them in the target) and the observed field gradients. The gradients lead

<sup>3</sup> The density of tungsten is 19.25 g/cm<sup>3</sup>, but more commonly admixtures of tungsten and Cu/Ni, or in this case tungsten powder, are used with somewhat lower densities<sup>531</sup>

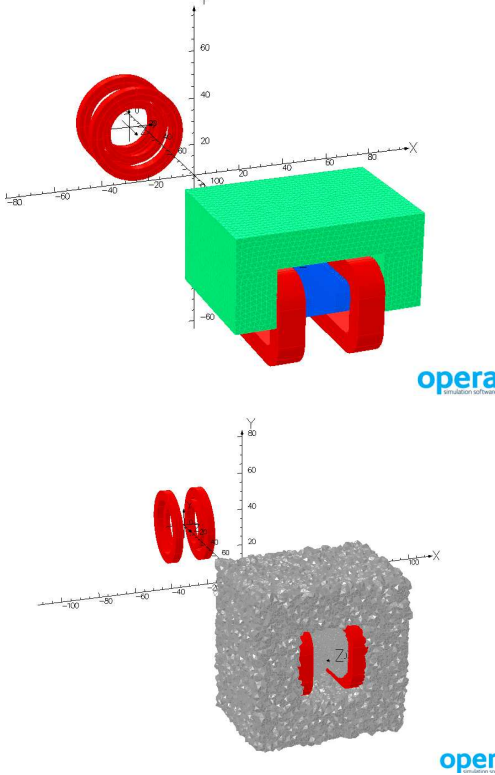


Figure 9: REMOVE "OPERA" FROM FIGURE. The TOSCA model used in the field and force calculations for longitudinal orientation of the coils/target polarization (top) and transverse orientation (bottom).

to about a 20-30 Gauss difference in  $B_x$ ,  $B_y$  at the locations of the two sets of coils (transverse to the beam direction). The force  $F_z$  (along the beam line) was found to be about 200 N, which is well below the recommended limit of 1000 N. This is the value that should be considered for support structure engineering designs. A similar force analysis for the polarized target magnet configured in a transverse (horizontal) orientation of the target field (see Figure 9 (right panel)) shows that the resulting force is slightly lower and the gradient at the target ( $B_x$  in this case) is around the same 2 Gauss/cm value.

## V Radiation Requirements

As discussed previously, the WACS experiment with the proposed CPS will utilize a dynamically nuclear polarized target. Electron beam currents for use with such targets are typically limited to 100 nA or less, to reduce both heat load and radiation damage effects. The equivalent heat load

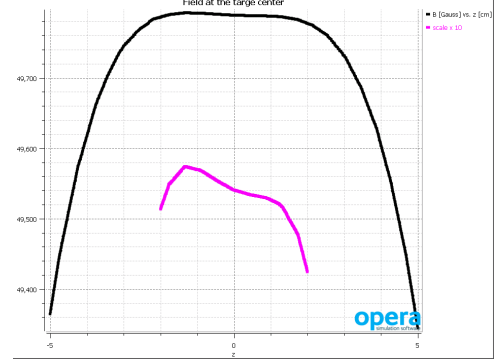


Figure 10: REMOVE "OPERA" FROM FIGURE. The field at the target center. Insert shows a field zoomed by a factor of 10. Values of the field (B) in Gauss and the coordinate (z) in cm. THIS CAPTION AND THE FIGURE NEEDS TO BE FIXED.

for a pure photon beam impinging on such a target corresponds to a photon flux originating from a  $2.7 \mu\text{A}$  electron beam current striking a 10% copper radiator. The radiation calculations presented in this section therefore assume a CPS able to absorb 30 kW in total (corresponding to a beam of 11 GeV electrons with a current of  $2.7 \mu\text{A}$ ). In addition, the beam time assumed for a typical CPS experiment is 1000 hours ( $\sim 40$  PAC days).

For such an experiment, the following radiation requirements must be fulfilled:

- The prompt dose rate in the experimental hall must be  $\leq$  several rem/hr at a distance of 30 feet from the CPS.
- The prompt dose rate at the site boundary must be  $\leq 1 \mu\text{rem}/\text{hr}$ . (For comparison,  $2.4 \mu\text{rem}/\text{hr}$  is the corresponding rate for a typical Jefferson Lab experiment which does not require extra shielding).
- The activation dose outside the CPS envelope at a distance of one foot must be  $\leq$  several mrem/hr one hour after the end of a 1000 hour run.
- The activation dose at the pivot in the experimental target area, where operational maintenance tasks may be required, is dominated by the dose induced by a pure photon beam, and at a distance of one foot from the scattering chamber must be  $\leq$  several mrem/hr one hour after the end of a 1000 hour run (i.e. the additional dose induced by radiation of the main beam absorbed in the CPS should be negligible).

585 The CPS design should combine in a single<sub>636</sub>  
 586 shielded assembly all elements necessary for the  
 587 production of the intense photon beam and ensure<sub>637</sub>  
 588 that the operational radiation dose rates are within  
 589 the requirements outlined above. Much of this is<sub>638</sub>  
 590 achieved by keeping the overall dimensions of the<sub>639</sub>  
 591 CPS as small as possible, by careful choice of ma-<sub>640</sub>  
 592 terials, and by locating radiation shielding as close<sub>641</sub>  
 593 to the source of radiation as possible. Compared<sub>642</sub>  
 594 to a traditional bremsstrahlung photon source, the<sub>643</sub>  
 595 proposed solution will present several advantages,<sub>644</sub>  
 596 including much lower radiation levels, both prompt<sub>645</sub>  
 597 and post-operational due to the beam line elements<sub>646</sub>  
 598 radio-activation, as will be shown later in this sec-<sub>647</sub>  
 599 tion.<sub>648</sub>

600 The CPS conceptual design has been estab-<sub>649</sub>  
 601 lished with extensive and realistic simulations. As<sub>650</sub>  
 602 validation of the simulation tools used, benchmark<sub>651</sub>  
 603 comparisons were made with GEANT3, GEANT4,<sub>652</sub>  
 604 FLUKA and DINREG. **NEED TO ADD REFERENCES FOR THESE**<sup>4</sup> After benchmark<sub>653</sub>  
 605 validation, an extensive series of radiation calcula-<sub>654</sub>  
 606 tions were performed in order to:<sub>655</sub>

- 608 • Determine the size and layout of the shield-<sub>656</sub>  
 609 ing around the magnet, and the choice of<sub>657</sub>  
 610 materials (copper, Cu-W alloy, concrete, bo-  
 611 rated plastic, etc.).<sub>658</sub>
- 612 • Determine the magnet field requirements in<sub>658</sub>  
 613 terms of peak field, gap size, and field length.<sub>659</sub>
- 614 • Determine the radiation levels on the magnet<sub>660</sub>  
 615 coils, and based on these results to identify<sub>661</sub>  
 616 radiation hardened materials that might be<sub>662</sub>  
 617 used in building the coils.<sub>663</sub>
- 618 • Determine the radiation levels on the polar-<sub>664</sub>  
 619 ized target electronics.<sub>665</sub>
- 620 • Determine the radiation levels directly adja-<sub>667</sub>  
 621 cent to the CPS as well as at the experimen-<sub>668</sub>  
 622 tal hall boundary.<sub>669</sub>

623 The logic behind the CPS hermetic shield-<sub>670</sub>  
 624 ing design is that radiation ( $\gamma, n$ ) from the source<sub>671</sub>  
 625 should be a few times less than from a photon beam<sub>672</sub>  
 626 interacting with the material of a polarized target.<sub>673</sub>  
 627 The CPS is designed to meet the radiation level<sub>674</sub>  
 628 requirements specified in Appendix 2 for an elec-<sub>675</sub>  
 629 tron beam current of  $2.7\mu\text{A}$  (30 kW), run time of<sub>676</sub>  
 630 1000 hours, and the photon source as close to the<sub>677</sub>  
 631 target as possible. The shielding design consists of<sub>678</sub>  
 632 tungsten powder and 10 cm of 30% borated plas-<sub>679</sub>  
 633 tic. The addition of the latter has considerable<sub>680</sub>  
 634 impact in reducing the neutron flux escaping the<sub>681</sub>  
 635 CPS, illustrated in Figure 14.<sub>682</sub>

---

683  
 684  
 685  
 4 Note that these codes calculate particle yields/s/cm<sup>2</sup>,  
 686 which have to be converted into the effective dose rate (in  
 687 rem/hr) using Fluence-to-Effective Dose conversion fac-  
 688 tors [11] taking into account an energy-dependence factor.<sub>689</sub>

## VI Radiation Studies and Shielding Design

In this section we will describe several different configurations for comparison, the first of which is the default situation for dynamically nuclear polarized targets in Hall C and elsewhere, which is that of a 100 nA incident electron beam. The second configuration corresponds to the equivalent photon flux created by a  $2.7 \mu\text{A}$  electron beam on a 10% copper radiator incident on the same polarized target system. In this scenario, we remove all the secondary particles generated in order that it mimics a pure and background-free photon beam. The third scenario is one with the CPS under the same conditions, a  $2.7 \mu\text{A}$  electron beam on a 10% copper radiator, for which all the radiation background is included in the simulation. In some cases we have simulated only the effect of the CPS, while in others the CPS and the target system combined are considered.

### A Prompt Radiation Dose without a Target

In order to help introduce the shielding concept of the CPS, we start by comparing the prompt radiation doses as calculated in a ring detector covering a radial range between 5 and 10 cm from the beam line. We first calculate the prompt dose originating from a  $2.7 \mu\text{A}$  electron beam hitting a 10% copper radiator a distance of 2.15 m upstream of the pivot. There is no target system in this simulation, which means that all prompt radiation originates from the interaction between the primary beam and the radiator. Figure 11 shows two-dimensional dose rates originating from photons only (top left), from neutrons only (top right), from all particles (bottom left), and the one-dimensional prompt radiation dose along the beam direction (bottom right). Obviously, except for the neutron contribution most of the prompt radiation is created along the beam direction. The prompt radiation levels reach roughly 40 rem/hr, of which only around 200 mrem/hr is in the form of gamma radiation and 10 mrem/hr from neutrons. The remaining and clearly dominant contribution are the charged electrons and positrons created, inducing further showers.

A striking difference is observed in the case of a  $2.7 \mu\text{A}$  electron beam incident on a 10% copper radiator as before, but now located within the CPS. Figure 12 illustrates the prompt radiation

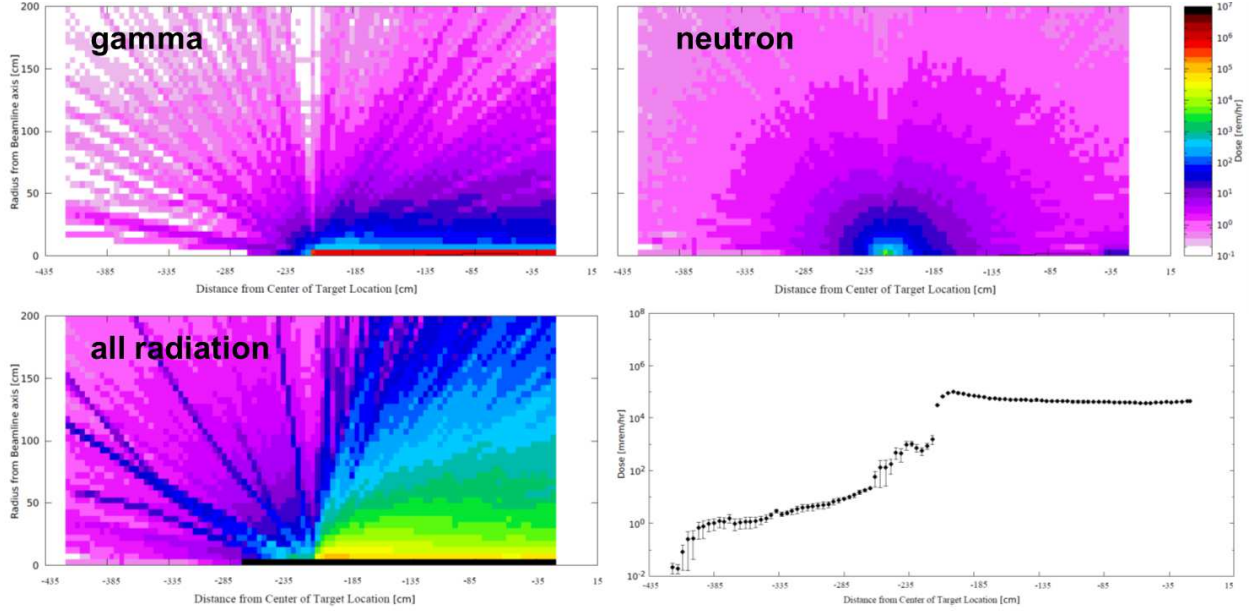


Figure 11: Two-dimensional dose rates as originating from photons only (top left), from neutrons only (top right), from all particles (bottom left) and the (one-dimensional) prompt radiation dose along the beam direction (bottom right).

686 dose along the beam direction. The y-axis scale<sup>716</sup>  
 687 on this figure is the same as in Figure 11 (bottom<sup>717</sup>  
 688 right panel). One can therefore clearly see that the  
 689 prompt radiation (again, in a 5 to 10 cm ring detec-  
 690 tor along the beam axis) within the CPS is much  
 691 higher (300 times, because with CPS the full power  
 692 of the beam is deposited). Crucially, however, the  
 693 prompt radiation dose outside the CPS is reduced  
 694 by a factor of over 1000 to roughly 15 mrem/hr.<sup>718</sup>  
 695 This factor is entirely consistent with the reduction  
 696 factor of estimated previously in section IV D.<sup>719</sup>

700     This extremely important result is further<sup>722</sup>  
 701 illustrated in Figure 13. In stark contrast with<sup>723</sup>  
 702 the case without the CPS, there is now no con-<sup>724</sup>  
 703 tribution to the prompt dose from photons, elec-<sup>725</sup>  
 704 trons and positrons – the neutron-only dose rate<sup>726</sup>  
 705 is nearly identical to the all-radiation rate. The<sup>727</sup>  
 706 fourth panel in Figure 13 (bottom right) illustrates<sup>728</sup>  
 707 how well an optimized CPS shielding concept ab-<sup>729</sup>  
 708 sorbs the prompt radiation. Outside the CPS the<sup>730</sup>  
 709 prompt radiation dose rate on the surface (indi-<sup>731</sup>  
 710 cated by the outer black rectangular lines) is re-<sup>732</sup>  
 711 duced to a maximum level of roughly 10 rem/hr.<sup>733</sup>  
 712 This shielding concept is so effective because of<sup>734</sup>  
 713 the fact that the development of showers gener-<sup>735</sup>  
 714 ated by interactions of the primary beam is highly<sup>736</sup>  
 715 suppressed and the resultant secondary particles<sup>737</sup>  
 716 contained. This confirms that with a CPS the fol-<sup>738</sup>  
 717 lowing requirement can be met: prompt dose rate<sup>739</sup>  
 718 in hall  $\leq$  several rem/hr at 30 feet from device.<sup>740</sup>

## B Impact of Boron and Shielding Optimization

718     It is well-known that the neutron flux  
 719 through a surface can be drastically reduced by  
 720 the addition of boron as a result of the very high  
 721 capture cross section of <sup>10</sup>B. We simulated this ef-  
 722 fect by calculating the neutron flux at the CPS  
 723 boundary assuming various thicknesses of tung-  
 724 sten shielding (65, 75 and 85 cm radial), and then  
 725 adding 10 cm of borated (30%) plastic. The result  
 726 can be seen in Figure 14, which shows the neutron  
 727 flux as function of neutron energy (on a logarithmic  
 728 scale). Adding 10 cm of tungsten clearly reduces  
 729 the neutron flux as expected, but a much more  
 730 drastic reduction is seen when the 10 cm of borated  
 731 plastic is added. Thus, in our design we assume an  
 732 outer layer of 10 cm-thick borated plastic for the  
 733 CPS. In order to demonstrate how well the shield-  
 734 ing design has been optimized, Figure 15 shows  
 735 a comparison between the prompt radiation dose  
 736 rates with the optimized shielding design (right)  
 737 and with 10 cm less tungsten shielding and no bo-  
 738 rated plastic (left). (Note that in these panels the  
 739 CPS magnet is assumed to be at the center of the  
 740 beam line, in contrast with earlier figures.)

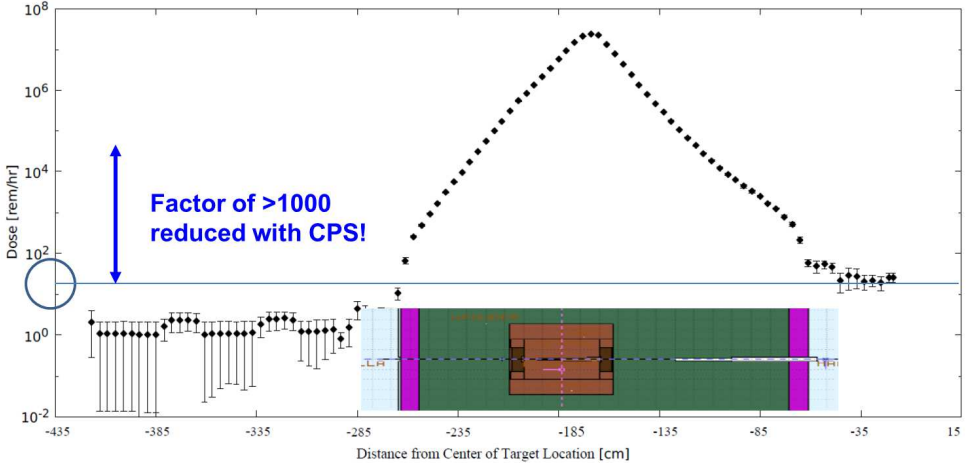


Figure 12: One-dimensional prompt radiation dose along the beam direction, from all particles. The large reduction factor of  $>1000$  induced by the Compact Photon Source design outside the magnet itself is apparent. Along the beam line inside the magnet, the prompt radiation dose can go up to above 10 Mrem/hr, dropping rapidly with distance.

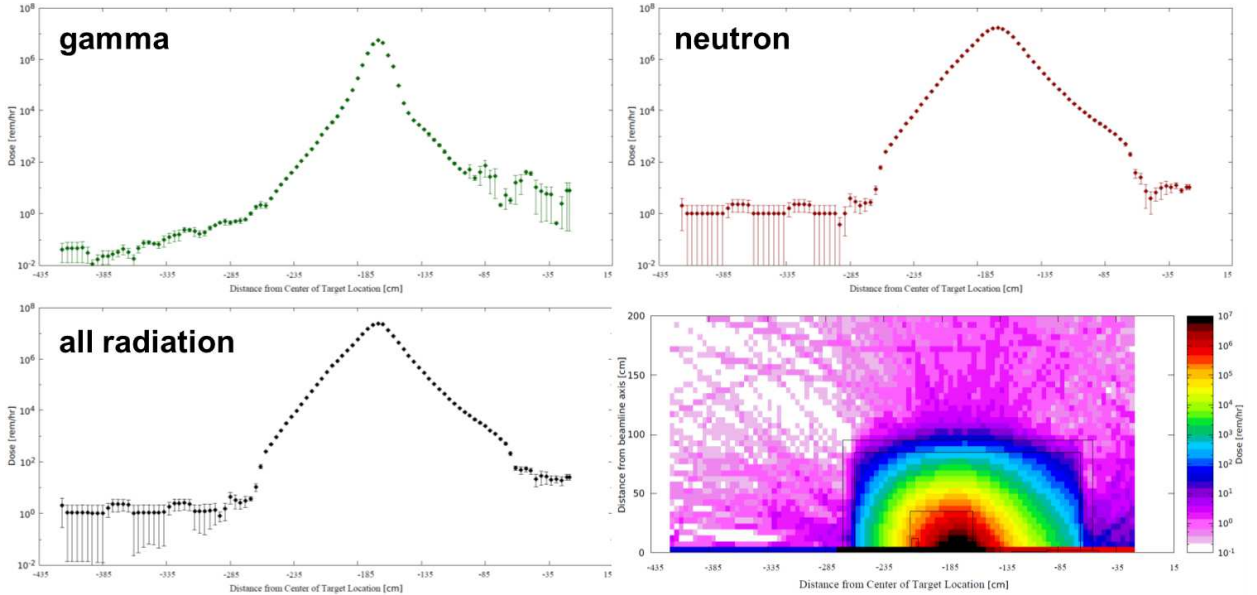


Figure 13: The (one-dimensional) prompt radiation rates as originating from photons only (top left), from neutrons only (top right), and from all radiation sources (bottom left). The fourth panel (bottom right) illustrates how well an optimized CPS shielding concept absorbs the prompt radiation, outside the CPS the prompt radiation is on the surface (indicated by the outer black rectangular lines) already reduced to a level of roughly 10 rem/hour at most.

## C Prompt Dose Rates at the Boundary

In benchmark calculations assuming spheres<sup>743</sup> of pure shielding materials (see a more extensive<sup>744</sup> description of the benchmark calculations in Ap-<sup>745</sup>pendix 2) we find that the prompt dose rate esti-<sup>746</sup>

<sup>747</sup>mates at the RBM-3 boundary are  $0.24 \mu\text{rem}/\text{hr}$  for a 3 meter diameter iron sphere and  $2.4 \mu\text{rem}/\text{hr}$  for a 1.5 meter diameter tungsten sphere. The baseline design for CPS shielding is assumed to be 85 cm thick tungsten surrounded by 10 cm of borated plastic. Hence, the boundary dose is below the  $2.4 \mu\text{rem}/\text{hr}$  that corresponds to a typical experimental run at Jefferson Lab, for which

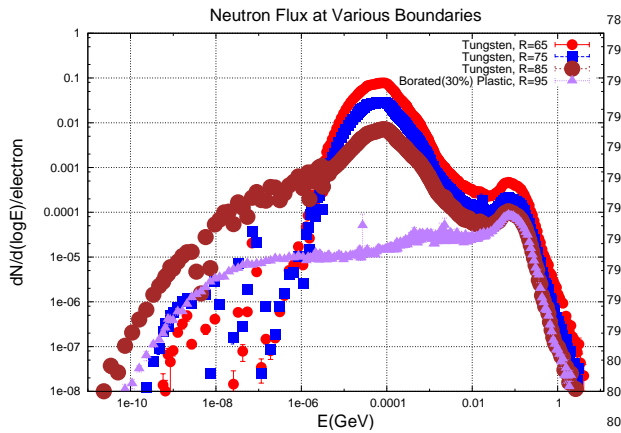


Figure 14: Neutron flux for different shielding configurationsB.

additional local shielding is not required. If required, further reductions in the boundary dose can be achieved by optimizing the baseline design in terms of material choice and geometry. Note also that for Hall D, the CPS design is compatible with the site boundary limits as the standard Hall D tagger magnet can dump up to 60 kW in a local beam dump. Indeed, the Hall D tagger building has been designed assuming a 12 GeV electron beam up to a current of 5  $\mu$ A. For the CPS, one can thus assume the Hall D tagger magnet building shielding is appropriate in the case for up to 60 kW being dumped in the CPS itself, albeit with the possibility that additional local shielding may be required.

## D Activation Dose without a Target

We now turn to the activation dose expected around the CPS following beam-on conditions. Figure 16 shows the calculated activation dose one hour after a 1000-hour experiment has been completed with the same conditions as before (2.7  $\mu$ A, 10% copper radiator, with shielded CPS). The radiation calculations show the activation dose outside the CPS is reduced to the order of roughly 1 mrem/hr. To quantify this further, Figure 17 shows the activation dose radially away from the CPS. The activation dose outside the CPS is reduced to 2 mrem/hr at the surface and reduces radially outward. At one-foot distance, it is reduced to about 1.5 mrem/hr, while at two-feet distance it is further reduced to less than 1 mrem/hr. Hence, this demonstrates that the current design meets the requirement that activation dose outside the

device envelope at one foot distance is  $\leq$  several mrem/h after one hour following the end of a 1000 hour run.

Note that these estimates do not depend much on the assumed 1000-hour continuous running assumption, as similar dose rates are seen in a calculation for a 100-hour continuous run, reflecting that much of the activation is instant. Furthermore, activation dose rates do not drop appreciably after one hour or even one day. On the other hand, after one month the activation dose rates at the CPS surface will be reduced by up to a factor of ten. Inside the CPS the activation dose rate can be up to 1 krem/hr, which is why the CPS will be moved laterally to the side after an experiment rather than disassembled.

## E Radiation Dose Rates with a Target

In building further on our radiation calculations, we have included the polarized target scattering chamber and target system. In Figure 18 we illustrate our setup and show a side-view of the CPS, indicating the magnet, the tungsten-powder shield, the layer of borated plastic, and also the scattering chamber with polarized target system. The description of the scattering chamber and polarized target includes: the exact diameter of the scattering chamber and all the ports with accurate dimensions and window materials; and the polarized target material including the liquid helium surrounding the target beads.

Figure 19 is included here for completeness. It illustrates the 1-MeV neutron equivalent damage to silicon (in neutrons/cm<sup>2</sup>), which is the relevant quantity to quantify the risk of radiation damage to sensitive electronics. The result, not surprisingly, shows that there is a narrow cone in the forward direction, along the beam axis, up to roughly one meter, in which sensitive electronics should not be placed if at all possible.

Figure 20 shows the prompt dose at the target for different configurations. The distance  $R$  is radial distance from the pivot, with the radius of the scattering chamber boundary at 50 cm. The various colors on the figure represent the various types of configurations studied: the 100 nA electron beam (red downward triangles), the 2.7  $\mu$ A photon beam (blue upward triangles), the CPS without polarized target (black circles), and the CPS with polarized target (mauve squares). At the boundary of the scattering chamber in the 100 nA electron beam configuration, the default operating

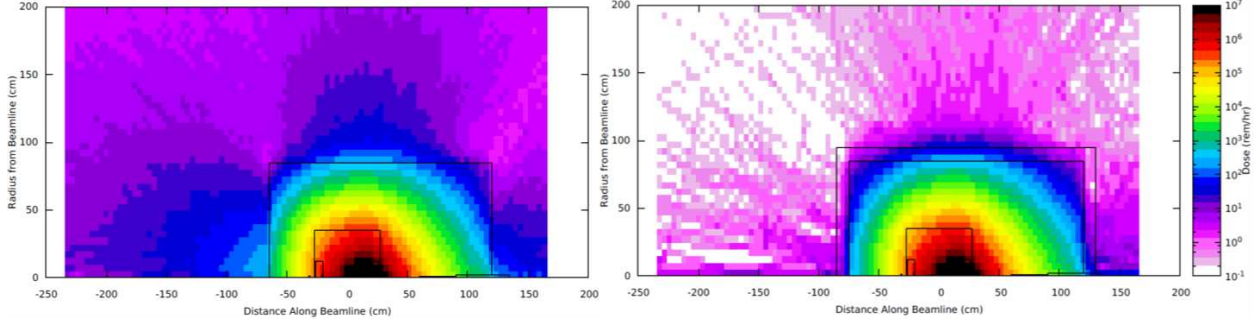


Figure 15: The prompt radiation rates with the optimized shielding design, whereas in the left panel we show the same prompt radiation rates without extra shielding (10 cm less of tungsten shielding, and no borated plastic). Note: these are with the CPS magnet centered around "zero" along the beam line.

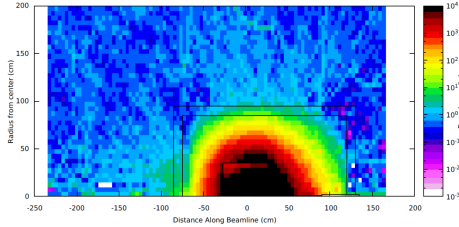


Figure 16: Calculated activation dose one hour after a 1000-hour experiment under the described conditions (2.7  $\mu$ A, 10% Cu radiator, with shielded CPS) has been completed. Note: these are with the CPS magnet centered around "zero" along the beam line.

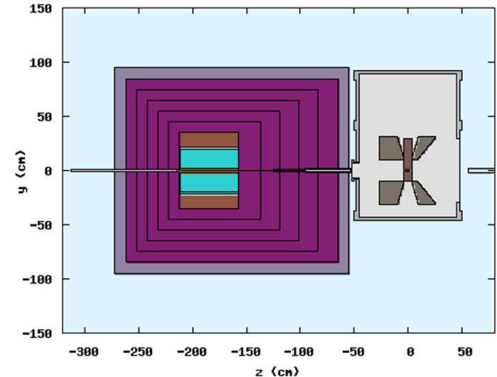


Figure 18: Side view of the Compact Photon Source, indicating the magnet, the W powder shield, and the layer of borated plastic, and also the scattering chamber with polarized target system.

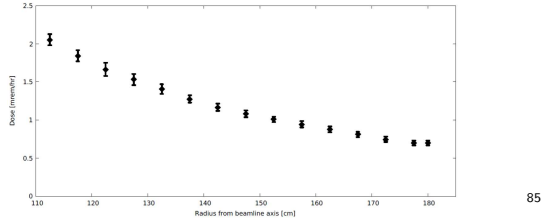


Figure 17: Activation dose outside CPS 1 hour after<sup>856</sup> a 1000 hour run is 2 mrem/hr on contact and reduced<sup>857</sup> radially outwards.  
<sup>858</sup>  
<sup>859</sup>  
<sup>860</sup>

mode for polarized beam experiments with dynamically nuclear polarized targets in Hall C to date,<sup>861</sup> the prompt dose is roughly 1 rem/hr. In the 2.7<sup>862</sup>  $\mu$ A *photon beam* scenario it is roughly 30 rem/hr,<sup>863</sup> which simply reflects the fact that even if a 2.7  $\mu$ A<sup>864</sup> pure photon beam deposits the same heat load in<sup>865</sup> a target as a 100 nA electron beam, the radiation<sup>866</sup> rate is much higher. The *CPS with polarized target*<sup>867</sup> scenario is identical to the pure photon beam case,<sup>868</sup> further demonstrating that no additional radiation<sup>869</sup> comes from the CPS.<sup>870</sup>  
<sup>871</sup>

Figure 21 is perhaps more instructive, in<sup>872</sup> that it shows the activation dose rates for the same<sup>873</sup>

three configurations. The vertical size of the figure panels have been adjusted such that equal dose rates line up from left to right. One directly can see therefore that the 2.7  $\mu$ A *photon beam* configuration has a much higher activation dose rate than the 100 nA *electron beam* case. This again reflects what was seen in the previous figure for the prompt radiation dose rate, as there are many more photons coming from a 2.7  $\mu$ A electron beam on a 10% copper radiator than there are from a 100 nA electron beam on a roughly 3% dynamically nuclear polarized target. More interestingly, the effect of the CPS is again negligible: activation near the target does not come from the CPS itself, but rather from the photon beam we have created. The price to pay is that one ends up with a roughly constant 0.1 mrem/hr activation level at large radial distances, but this is manageable.  
<sup>874</sup>

We also indicate in the various panels of Figure 21 how quickly the activation rates drop (after

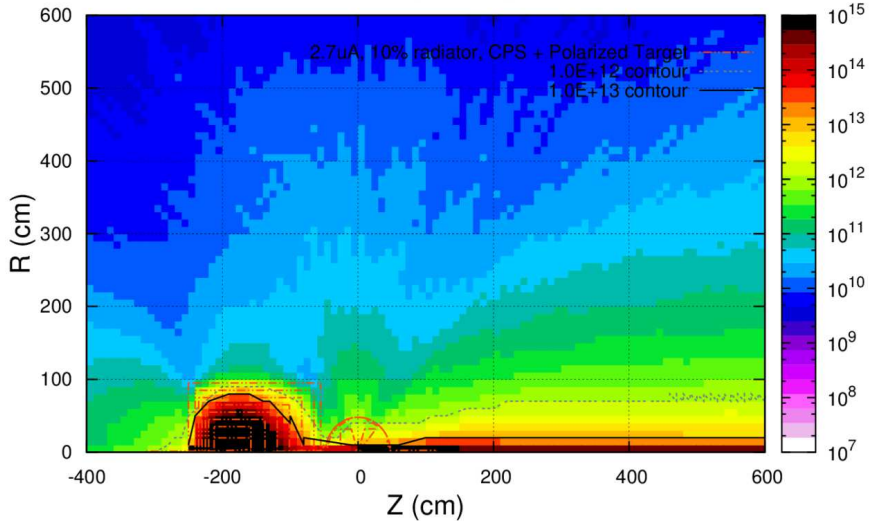


Figure 19: 1-MeV neutron equivalent damage to silicon (in neutrons/cm<sup>2</sup>).

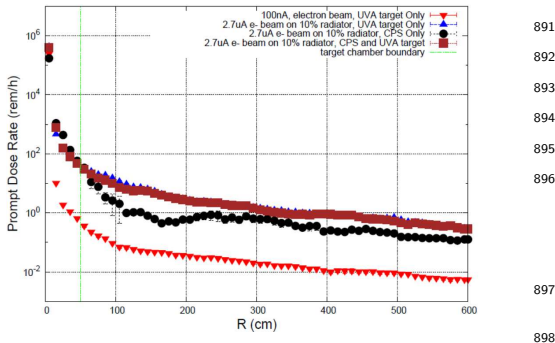


Figure 20: Prompt dose at the target for different configurations. Distance  $R$  is radial distance from the pivot, with the radius of the scattering chamber bound-  
ary at 50 cm.

one hour, one day, one week, and one month). One can see that much of the 0.1 mrem/hr activation level induced by the deployment of the CPS has decayed away after a week. This is consistent with what was observed in the example of the activation levels at radial distances around the CPS above.

Finally, we illustrate in Figure 22 in a two-dimensional plot the activation dose rates one hour after a 1000 hour run with the CPS, a  $2.7 \mu\text{A}$ , 11 GeV beam on a 10% radiator and the polarized target system (at  $z = 0$ ). The 1 mrem/hour contour is indicated. This demonstrates that with the current CPS baseline design, the activation dose at the pivot in the experimental target area, where operational maintenance tasks may be required, is dominated by the dose induced by a pure photon beam and is at one-foot distance from the scatter-

ing chamber  $\leq$  several mrem/hr one hour after a 1000 hour run, and also that **the additional dose induced by radiation of the main beam absorbed in the CPS is negligible**. This fulfills the last of the radiation requirements that were introduced in section V.

## VII Engineering and Safety Aspects

In this section we will describe the engineering and safety aspects of the CPS. We will start with a summary of material considerations taking into account the high radiation and power inside the CPS, folding in further insights of the radiation studies as relevant for materials for the CPS and the dynamically nuclear polarized target. Then we describe various engineering aspects such as cooling and magnetic forces, and some further considerations for assembly and installation of the CPS. We will also shortly outline safety aspects related to the CPS, such as use of interlock systems during CPS operation.

### A Material Considerations

The level of radiation of the CPS experiments is well below what is typical for many high-luminosity experiments in Experimental Halls A and C at Jefferson Lab using regular cryogenics target systems and/or radiators. The prompt ra-

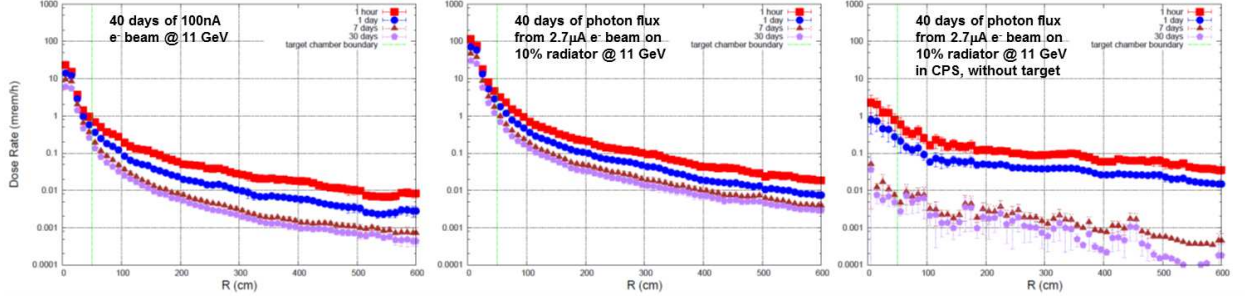


Figure 21: Activation dose rates at the target for different configurations. Distance  $R$  is radial distance from the pivot, with the radius of the scattering chamber boundary at 50 cm.

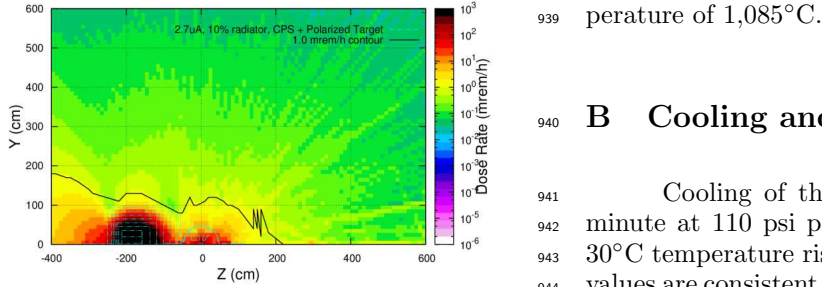


Figure 22: Activation dose rates one hour after a 1000-hour run with the Compact Photon Source, a  $2.7 \mu\text{A}$  beam and a 10% radiator, at 11 GeV beam energy, and the polarized target system (at  $z = 0$ ). The 1  $\text{mrem}/\text{hr}$  contour is indicated. Note that these activation dose rates do not depend much on the assumed 1000-hour continuous run, the rates would be only slightly lower (by 5-10%) and near-identical for a 100-hour continuous run, after one hour.

diation level on the polarized target is higher than before, which is simply an artefact of the higher photon flux associated with the higher figure-of-merit of the CPS experiments. The radiation level on the polarized target coils, due to the interaction of the photon beam with the polarized target material, amounts to about 500 rem/hr as illustrated in Figure 23. The radiation levels in the CPS magnet coils, at a distance of 20 cm from the radiation source, are reduced to below 1 Mrem/hr (see e.g. Figure 13, bottom right), and allow the use of modest-cost Kapton tape-based insulation of the coils [12].

As described in Section IV B, we explicitly added a small insert of copper within the tungsten-powder shielding of CPS to act as the beam power absorber. The combination of a small  $\pm 1$  mm vertical raster and the magnet field shaping spreads the beam power density over a large surface, such that the temperature of the copper absorber was less than  $400^\circ\text{C}$ . This is well below its melting tem-

perature of  $1,085^\circ\text{C}$ .

## B Cooling and Magnetic Forces

Cooling of the core requires 4 gallons per minute at 110 psi pressure. This will result in a  $30^\circ\text{C}$  temperature rise of the cooling water. These values are consistent with provisions in Experimental Hall C at Jefferson Lab, the Hall planned for use for the approved CPS science program. Activation of the cooling water of the CPS magnet and beam dump is likely and a closed-cycle cooling system is planned. Hall C has had secondary in-Hall water-cooled dumps of comparable power before, for polarized target experiments in the 6-GeV era. High-power radiators are also not new and have been used with tens of  $\mu\text{A}$  on 10% radiation length targets, also with closed-loop water cooling systems. The magnet heat and dump heat can be removed through a heat exchanger to either the Hall C air or LCW. Any activation of the CPS will be confined to a very small volume and in the event of a leak external contamination will be minimized. A leak pan under the CPS could easily be included to catch and confine any leakage up to and including a total loss of primary coolant. A modular pallet mounted design would be efficient and would include primary coolant pumps, DI resin beds, heat exchanger, surge tank, controls, and instrumentation and manifolds.

The CPS magnet will be located relatively close to the 5 Tesla solenoid of the polarized target whose mutual forces need to be taken into account in the design of the support structure and may require compensation. Preliminary analysis was already performed in a technical note, at that time based on iron-based shielding [13]. In the present design the iron-based shielding is replaced by more effective tungsten-powder shielding, which also much reduces the forces. Residual fields and

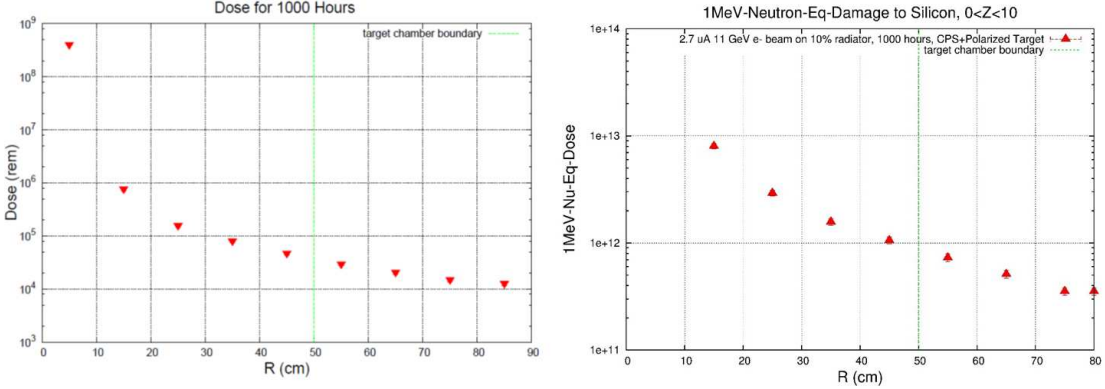


Figure 23: The prompt dose rates (right) and the resulting 1 MeV neutron equivalent damage to silicon (left) in the target area, assuming a 1000 hour run with the Compact Photon Source with a 2.7 mA beam, a 10% Cu radiator, and 11 GeV beam energy. The polarized target system is at  $z = 0$  and the nominal target chamber radius is 50 cm. The target coils are at about 20 cm from the beam line. The dose for 1000 hours of beam time at the target coils is 5 times  $10^5$  rem and the 1 MeV neutron equivalent damage is 5 times  $10^{12}$  neutrons/cm $^2$ . The contribution of the CPS backgrounds to these numbers is negligible (contributing 2.5% only).

977 forces from the CPS magnet will require further<sup>1008</sup>  
 978 iron shielding to avoid interference with the Polar<sup>1009</sup>  
 979 ized Target magnet.<sup>1010</sup>

980 Another magnetic consideration is the effect<sup>1011</sup>  
 981 on field quality at the polarized target. The fields<sup>1012</sup>  
 982 and gradients imposed on the polarized target will<sup>1013</sup>  
 983 not be large but they must be compensated at the<sup>1014</sup>  
 984  $10^{-4}$  level. Some further magneto-static effort<sup>1015</sup>  
 985 to model the target environment and design a com<sup>1016</sup>  
 986 pensation system is required.<sup>1017</sup>

## 987 C Assembly and Installation 988 Considerations<sup>1018</sup>

989 The CPS can be completely pre-assembled<sup>1024</sup>  
 990 before installation. The outer dimension of the<sup>1025</sup>  
 991 CPS tungsten-powder shielding as outlined for op<sup>1026</sup>  
 992 timized shielding (see Figure 15, right panel) is<sup>1027</sup>  
 993 1.7 m by 1.7 m by 1.95 m, or a volume of  $5.63 \text{ m}^3$ <sup>1028</sup>  
 994 From this, one needs to subtract the inner box in<sup>1029</sup>  
 995 cluding the magnet, which amounts to  $0.26 \text{ m}^3$ <sup>1030</sup>  
 996 This means a net volume of  $5.37 \text{ m}^3$ , or 88 tons<sup>1031</sup>  
 997 for the optimized tungsten-powder shielding pre<sup>1032</sup>  
 998 sented. In total, the CPS weight is estimated t<sup>1033</sup>  
 999 be 100 tons. Hence, a reinforced floor would b<sup>1034</sup>  
 1000 required for CPS assembly.<sup>1035</sup>

1001 There are various options to reduce weight<sup>1036</sup>  
 1002 and cost, as needed. Note that the cost of the CPS<sup>1037</sup>  
 1003 will be dominated by the cost of the shielding ma<sup>1038</sup>  
 1004 terials. One could reduce the overall size of the W<sup>1039</sup>  
 1005 powder shielding by 5 cm on each side. This would<sup>1040</sup>  
 1006 imply an increase of the radiation levelswe esti<sup>1041</sup>  
 1007 mated by about 50%, and a reduction to  $4.48 \text{ m}^3$ <sup>1042</sup>

or 73 tons (for the W-powder). If one would remove an additional 10 cm only on the bottom side, towards the floor, for an additional factor of two increase in radiation level in the direction of the floor, as calculated for the example of Experimenatl Hall C at Jefferson Lab, this reduces to 68 tons. Alternatively, one could round the W-powder box corners, as illustrated in Figure 24. This would complicate modular construction, but would allow to reach similar radiation levels aas with the optimized design, while reducing material needs and weight. To verify this, we updated the FLUKA model originally developed by one of us (Parker Reid (SMU)) to assist the CPS conceptual design, and replaced the W-powder ( $\rho = 16.3 \text{ g/cm}^3$ ) with B(5%)-CH<sub>2</sub> in the rounded corners. The result of the FLUKA analysis confirmd that such a configuration can achieve the same level of radiation outside of the CPS as the optimized shielding design model, but with the volume (and weight) of the W-powder reduced by 25%, to  $\approx 66$  tons.

During assembly and after assembly completion the CPS can be measured and fiducialized to facilitate final alignment. Progressive measurement and fiducialization will eliminate problems with position references becoming hidden. Transporting the CPS to (or within) an Experimental Hall in one piece will preserve the alignment and avoids introduction of errors due to dis-assembly and re-assembly, albeit require temporary use of a large 100-ton truck crane.

When in use for is science experiments, the CPS is expected to become activated and contaminated. Activation levels inside the CPS are ex-  
 pected to be and remain high, until well after ex-

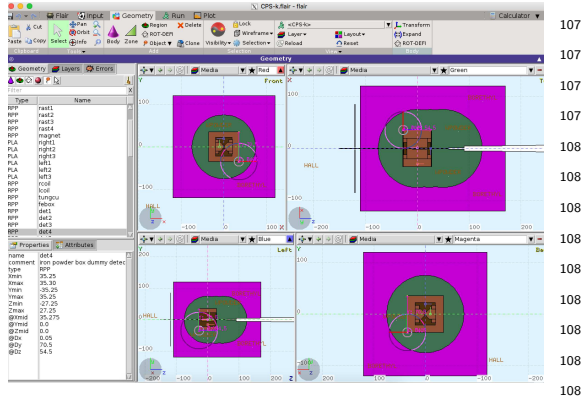


Figure 24: NEED BETTER FIGURE. The FLUKA<sup>1089</sup> model used in calculations of radiation. Here, front,<sup>1090</sup> back, right and left views are shown, illustrating the<sup>1091</sup> rounded W-powder (green) corners and the outer bo<sup>1092</sup> rated plastic (purple) volume.

periment completion. Hence, designing the CPS<sub>1096</sub> for a one-piece removal limits exposure to staff at<sub>1097</sub> the end of the experiments. The CPS can be left<sub>1098</sub> in place, or if removal is required, this task would<sub>1099</sub> again require one-time use of a large truck crane to<sub>1100</sub> handle the total 100-ton weight of the CPS. The<sub>1101</sub> CPS can then be stored. This eliminates the need<sub>1102</sub> for staff to dis-assemble the CPS.

Water disconnects using self-sealing connectors<sub>1104</sub> can be used to eliminate any primary cooling<sub>1105</sub> water loss. The cooling water pumps, controls, DI<sub>1106</sub> resin beds and heat exchanger will likely have con<sub>1107</sub> taminated water inside but will not otherwise be<sub>1108</sub> activated. The cooling pallet can be removed to<sub>1109</sub> storage intact or the water drained and stored sep<sub>1110</sub> arately or disposed of. The radiator infrastructure<sub>1111</sub> can be similarly stored.

## 1060 D Equipment Safety and Interlocks

1061 The combination of a high-power radiator,  
1062 magnet and beam dump inside a shielded box  
1063 impose reliability and remote handling considera<sub>1115</sub>  
1064 tions. The primary engineering controls provid<sub>1116</sub>  
1065 ing personnel protection are to make the design as<sub>1117</sub>  
1066 robust as possible, with large safety margins, and<sub>1118</sub>  
1067 evade disassembly for maintenance and repair, or<sub>1119</sub>  
1068 equipment removal, altogether.

1069 The CPS should be heavily instrumented for<sub>1121</sub>  
1070 early detection of problems such as low coolant<sub>1122</sub>  
1071 flow, leaks, low pressure, high temperature, and<sub>1123</sub>  
1072 high conductivity. The protection and safety of the<sub>1124</sub>  
1073 CPS begins with the design which must err on the<sub>1125</sub>  
1074 side of conservatism especially in the magnet coil<sub>1126</sub>  
1075 design and dump cooling. A low current density<sub>1127</sub>

1076 design is envisioned, not to exceed 500 Amps/cm<sup>2</sup>.  
1077 Individual coil pancakes leads should be extended  
1078 to an area outside of the magnet and shielding  
1079 for easy access. There should be no electrical or  
1080 coolant joints inside the CPS shielding. Every sepa-  
1081 rate sub coil of the CPS magnet should have ther-  
1082 mometry, klixons and flow measurements to avoid  
1083 any possibility that one of the separate current  
1084 paths can overheat due to lack of sufficient coolant,  
1085 a leak or a bad electrical joint. Voltage monitoring  
1086 of each sub coil should insure against overheating  
1087 from any source including internal blockage, leaks,  
1088 flow restrictions or bad electrical connections. Ex-  
1089 tra insulation between sub coils and between the  
1090 coil and ground should be added to prevent ground  
1091 faults. Lastly, a commercial power supply is as-  
1092 sumed and these come with a wide array of inter-  
1093 lock protections. The available interlocks and signals  
1094 can be fed into an electron beam Fast  
1095 Shutdown (FSD) system.

To protect equipment during CPS operations, a dual protection scheme is suggested using both a beam position monitoring system and direct instrumentation of the fast raster magnet itself. The beam diagnostics systems would monitor beam position and motion in close to real time and monitor cold voltage on the raster coils, which would provide ample early warning of raster problems. Both these independent signals would be fed into the FSD system. Radiator temperature could be monitored to provide a third independent protection system, and if implemented, thermocouples mounted on the radiator should be robust against radiation damage and provide fast enough protection against radiator overheating. Simulations of various magnet failure modes such as reduced or no water flow, overheating, etc., can be used to proof test instrumentation and interlocks.

## 1114 VIII Summary

The Compact Photon Source (CPS) design features a magnet, a central copper absorber and hermetic shielding consisting of tungsten powder and borated plastic. The addition of the latter has a considerable impact on reducing the neutron flux escaping the CPS. The ultimate goal in this design process is that radiation from the source should be a few times less than from a photon beam interacting with the material of a polarized target. The equivalent heat load for a pure photon beam impinging such targets corresponds to a photon flux originating from a  $2.7 \mu\text{A}$  electron beam current striking a 10% copper radiator. Detailed simula-

tions of the power density and heat flow analysis show that the maximum temperature in the absorber is below 400 degrees, which is well within the acceptable range of copper, and thus demonstrates that the CPS can absorb 30 kW in total e.g. corresponding to an 11-GeV electron beam energy and a 2.7  $\mu$ A electron beam current.

The CPS also fulfills the requirements on operational dose rates at Jefferson Lab, which have been established with extensive and realistic simulations. The projected prompt dose rate at the site boundary is less than 1  $\mu$ rem/hr (to be compared with 2.4  $\mu$ rem/hr, which corresponds to a typical JLab experiment that does not require extra shielding). The activation dose outside the device envelope at one foot distance is less than several mrem/hr after one hour following the end of a 1000 hour run ( $\sim$  3 months). The activation dose at the pivot in the experimental target area, where operational maintenance tasks may be required, is dominated by the dose induced by the pure photon beam. At a distance of one foot from the scatter chamber it is less than several mrem/hr one

hour after the end of a 1000 hour run (i.e. the additional activation dose induced by absorption of the electron beam in the Compact Photon Source is negligible).

This document demonstrates that the CPS with an optimized shielding design provides a photon flux of  $1.5 \times 10^{12}$  equivalent photons/s, with a factor of 1000 reduction in prompt radiation dose compared to a 2.7  $\mu$ A (30 kW) electron beam current striking a 10% copper radiator. The CPS meets the acceptable radiation level requirements for a typical run time of 1000 hours with the photon source located at 2 m from the target. The technical design and installation in the current hall infrastructure is feasible.

## IX Acknowledgements

We thank Paul Brindza for helpful discussions and providing valuable input for the writing of this document.

- 
- [1] M.J. Amaryan, M. Bashkanov, S. Dobbs, J. Ritman, J.R. Stevens, and I.I. Strakovsky, and the KLF Collaboration, Jefferson Lab Experiment C12-19-001.
  - [2] D. Hamilton, D. Day, D. Keller, G. Niculescu, B. Wojtsekowski, J. Zhang, and the Neutral Particle Spectrometer Collaboration, Jefferson Lab experiment E12-17-008.
  - [3] M. Boer, D. Keller, V. Tadevosyan, and the Neutral Particle Spectrometer Collaboration Jefferson Lab experiment C12-18-005.
  - [4] E. Chudakov, D. Day, P. Degtiarenko, R. Ent, D.J. Hamilton, T. Horn, D. Keller, C. Keppel, G. Niculescu, P. Reid, I. Strakovsky, B. Wojtsekowski, and J. Zhang, Compact Photon Source Conceptual Design, (2018). Available online [https://wiki.jlab.org/cuawiki/images/4/4f/CPS\\_document\\_rev9.pdf](https://wiki.jlab.org/cuawiki/images/4/4f/CPS_document_rev9.pdf)
  - [5] R.L. Anderson et al., Physical Review Letters, **25**, no. 17 (1970), 1218; R.L. Anderson et al., Physical Review D, **14**, no. 3 (1976), 679; G.E. Fischer et al., Nucl. Inst. and Meth. **78** (1970), 25; Y.S. Tsai and V. Whitis, Physical Review, **149**, no. 4 (1966), 1248.
  - [6] N.R.S. Tait, Nuclear Instruments and Methods **67** (1969) 56; T.A. Armstrong et al., Physical Review D, Volume **5**, Number 7, (1972); A. Jackson, Nuclear Instruments and Methods **129** (1975) 73.
  - [7] G.R. Court et al., Nuclear Instruments and Methods **177** (1980) 281.
  - [8] G.G. Crabb, W. Meyer, Ann. Rev. Nucl. Part. Sci. **47** (1997) 67.
  - [9] B. Wojtsekowski, D. Day, et al., PR05-101 (2005); P. Achenbach et al., MAMI-C.
  - [10] W.P. Swanson, SLAC-PUB 2042 (1977); unpublished.
  - [11] ICRP, 2010. Conversion Coefficients for Radiological Protection Quantities for External Radiation Exposures. ICRP Publication 116, Ann. ICRP 40(25).
  - [12] V.V. Petrov, Yu.A. Pupkov, a report “BINP TESTING OF RADIATION RESISTANCE OF THE MATERIALS USED FOR PRODUCTION OF ACCELERATOR MAGNETIC SYSTEMS”, document Novosibirsk, 2011
  - [13] B. Wojtsekowski and G. Niculescu, “Conceptual Design Report, A Compact Photon Source”, Supplementary material for the WACS proposal PR12-15-003 to the JLab PAC 43, June 2015; in arXiv:1704.00816.  
M. Wiseman, C.K. Sinclair, R. Whitney, M. Zarecky, “High Power Electron Beam Dumps at CEBAF”.